

Range dependence of the response of a spherical head model

Richard O. Duda

Department of Electrical Engineering, San Jose State University, San Jose, California 95192

William L. Martens

Human Interface Lab, University of Aizu, Aizu-Wakamatsu 965-80, Japan

(Received 28 July 1997; revised 1 July 1998; accepted 2 July 1998)

The head-related transfer function (HRTF) varies with range as well as with azimuth and elevation. To better understand its close-range behavior, a theoretical and experimental investigation of the HRTF for an ideal rigid sphere was performed. An algorithm was developed for computing the variation in sound pressure at the surface of the sphere as a function of direction and range to the sound source. The impulse response was also measured experimentally. The results may be summarized as follows. First, the experimental measurements were in close agreement with the theoretical solution. Second, the variation of low-frequency interaural level difference with range is significant for ranges smaller than about five times the sphere radius. Third, the impulse response reveals the source of the ripples observed in the magnitude response, and provides direct evidence that the interaural time difference is not a strong function of range. Fourth, the time delay is well approximated by well-known ray-tracing formula due to Woodworth and Schlosberg. Finally, except for this time delay, the HRTF for the ideal sphere appears to be minimum-phase, permitting exact recovery of the impulse response from the magnitude response in the frequency domain.

© 1998 Acoustical Society of America. [S0001-4966(98)00111-8]

PACS numbers: 43.66.Qp, 43.66.Pn 43.20.Fn [RHD]

LIST OF SYMBOLS

a	radius of the sphere (m)
c	ambient speed of sound (m/s)
f	frequency (Hz)
h	head-related impulse response
h_m	m th-order spherical Hankel function
h'_m	the derivative of h_m with respect to its argument
H	head-related transfer function relative to free field
H_e	head-related transfer function relative to source
i	$\sqrt{-1}$
j_m	m th-order spherical Bessel function
k	acoustic wave number (/m)
n_m	m th-order spherical Neumann function
p_{ff}	free-field pressure at the center of the sphere (kg/m^2)
p_s	pressure on the surface of the sphere (kg/m^2)
p_e	pressure at a small sphere surrounding the source (kg/m^2)

P_m	Legendre polynomial of degree m
Q_m	m th-order modified spherical Hankel function
r	distance from the center of the sphere to the source (m)
r_e	radius of a small sphere surrounding the source
S_ω	magnitude of flow from an ideal point source (m^3/s)
t	time (s)
Δt	time between arrival at observation point and sphere center (s)
$\Delta \tau$	normalized Δt
θ	angle of incidence (rad)
θ_0	angle for tangent incidence (rad)
λ	wavelength (m)
μ	normalized frequency
ρ	normalized distance to the source
ρ_0	density of air (kg/m^3)
τ	normalized time
ω	radian frequency (rad/s)

INTRODUCTION

This paper is concerned with the range dependence of the response of an ideal rigid sphere to a point sound source. The purpose of this study was to gain a better understanding of the behavior of the head-related transfer function (HRTF) at close range. It is hoped that these results will serve as a guide to those engaged in the study of human HRTFs, including their measurement and analysis, and to those engaged in creating spatial sound stimuli by convolving audio signals with these HRTFs. Given the paucity of experimental measurements of HRTF variation at close range, it seemed particularly important to have a foundation upon which to base further acoustical studies of this spatial region. There-

fore, the investigation reported in this paper included the numerical evaluation of a theoretical model, the collection of related acoustical measurement data, and the comparison of the theoretical solution to the experimental results.

A classical spherical model of the human head was chosen for this investigation for the traditional reasons—its response can be analyzed mathematically, and the theoretical solution can be evaluated numerically. Even though this model is quite idealized, it exhibits features similar to those observed in the close-range behavior of the human HRTF. For example, sounds from a source that is very close to one's ear are not only louder but also contain relatively more low-frequency energy than do sounds from a distant source. The

simplest model that explains these effects approximates the human head by a rigid sphere of the same average radius and approximates the sound impinging on the sphere as if it were generated by a point source. While this idealization is restricted to relatively low frequencies and obviously becomes problematic very close to the surface of the head, a quantitative understanding of its behavior provides insight into the more complex behavior of the HRTF for an actual human head.

To compute the response at the surface of the sphere for a sound source located at an arbitrary distance from the surface of the sphere, a modification was made to an algorithm for computing the classical solution for a source infinitely far from the sphere. The behavior of the solution was examined in both the frequency domain (the HRTF) and the time domain (the head-related impulse response, or HRIR). The time-domain solution provides insight into some otherwise puzzling behavior of the HRTF. The adequacy and accuracy of the model were confirmed by comparing the numerical results with the results of a corresponding series of impulse response measurements made using an actual physical sphere.

I. THE THEORETICAL SOLUTION

A. Expansion in spherical harmonics

The frequency-domain solution for the diffraction of an acoustic wave by a rigid sphere, which is presented in many textbooks, was obtained by Lord Rayleigh at the end of the 19th century (Strutt, 1904, 1945). If the flow for a complex sinusoidal point source is of the form $S_\omega e^{-i\omega t}$, then the free-field pressure at a distance r from the source is given by

$$p_{ff}(r, \omega, t) = -i\omega \frac{\rho_0 S_\omega}{4\pi r} e^{i(kr - \omega t)}, \quad (1)$$

where $k = \omega/c$.¹ Because multiplication by $-i\omega$ in the frequency domain is equivalent to differentiation in the time domain, this implies that if the flow is a unit step function, the free-field pressure is a Dirac impulse wave whose strength varies inversely with the distance to the source.

The presence of the sphere diffracts the sound wave and modifies the pressure field. Most authors give only Rayleigh's solution for the case where the source is infinitely distant from the center of the sphere. Rabinowitz *et al.* (1993) present the solution for the pressure on the surface of the sphere due to a sinusoidal point source at any range r greater than the sphere radius a . With minor notational changes, their solution can be written as

$$p_s(r, a, \omega, \theta, t) = \frac{i\rho_0 c S_\omega}{4\pi a^2} \Psi e^{-i\omega t}, \quad (2)$$

where Ψ is the infinite series expansion

$$\Psi = \sum_{m=0}^{\infty} (2m+1) P_m(\cos \theta) \frac{h_m(kr)}{h'_m(ka)}, \quad r > a. \quad (3)$$

Here θ is the angle of incidence, the angle between the ray from the center of the sphere to the source and the ray to the measurement point on the surface of the sphere, and normal

incidence corresponds to $\theta = 0^\circ$. It is conventional to use the time $2\pi a/c$ that it takes for a wave to travel once around the sphere to define the normalized frequency μ ,

$$\mu = ka = f \frac{2\pi a}{c}. \quad (4)$$

Define the normalized distance to the source ρ by

$$\rho = \frac{r}{a}, \quad (5)$$

and define the transfer function H by

$$H = \frac{P_s}{P_{ff}}. \quad (6)$$

Then

$$H(\rho, \mu, \theta) = -\frac{\rho}{\mu} e^{-i\mu\rho} \Psi, \quad (7)$$

where

$$\Psi(\rho, \mu, \theta) = \sum_{m=0}^{\infty} (2m+1) P_m(\cos \theta) \frac{h_m(\mu\rho)}{h'_m(\mu)}, \quad \rho > 1. \quad (8)$$

This "head-related transfer function" H relates the pressure that would be present at the center of the sphere in free field to the pressure that is actually developed at the surface of the sphere.² The inverse Fourier transform of H is the normalized "head-related impulse response" h [which should not be confused with the m th-order spherical Hankel function h_m in Eq. (8)].

B. Limiting cases

The behavior of the transfer function as the normalized range ρ becomes arbitrarily large can be obtained by using the asymptotic formula (see Morse and Ingard, 1968, Chap. 7.2)

$$h_m(x) = j_m(x) + i n_m(x) \rightarrow \frac{e^{i(x - [(m+1)/2]\pi)}}{x}. \quad (9)$$

This leads to

$$H(\infty, \mu, \theta) = \frac{1}{\mu^2} \sum_{m=0}^{\infty} \frac{(-i)^{m-1} (2m+1) P_m(\cos \theta)}{h'_m(\mu)}, \quad (10)$$

which is Rayleigh's solution for an infinitely distant source. The low-frequency behavior can be obtained from the first two terms in this series, which leads to the well-known result

$$H(\infty, \mu, \theta) \approx 1 - i \frac{3}{2} \mu \cos \theta. \quad (11)$$

Thus, at low frequencies, the magnitude of H is essentially unity, and the phase angle is approximately $-\frac{3}{2} \mu \cos \theta$, which corresponds to a group delay of $-\frac{3}{2} a \cos \theta/c$ (Kuhn, 1977).

Since both Eqs. (8) and (10) converge more and more slowly as μ increases, the high-frequency behavior is less obvious. Kuhn (1977) obtained the high-frequency solution by employing an alternative "creeping wave" expansion.

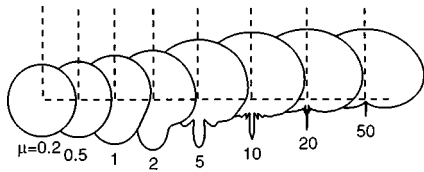


FIG. 1. Polar plots of the magnitude of the transfer function for an infinitely distant source. A bulge in the response starts to become distinct when the normalized frequency is around 1, i.e., when the wavelength equals the circumference of the sphere. As the frequency increases, the response at the front of the sphere approaches twice the free-field response. In addition, the response on the shadowed side of the sphere becomes progressively smaller, except for the celebrated “bright spot” at the back of the sphere.

For the special case of normal incidence ($\theta=0$ degrees), one can argue on physical grounds that when the wavelength is small compared to the radius of the sphere, the solution must reduce to that of a plane wave normally incident on a rigid plane surface, where the pressure at the surface becomes twice the free-field pressure. Thus,

$$|H(\infty, \infty, 0)| = 2. \quad (12)$$

These special case results serve to define interesting limits of the general solution.

II. BEHAVIOR OF THE THEORETICAL SOLUTION

A. Frequency response—distant range

In general, one must use numerical methods to evaluate the transfer function $H(\rho, \mu, \theta)$ for arbitrary values of ρ , μ and θ . Bauck and Cooper (1980) developed a simple but effective algorithm for evaluating the solution for an infinitely distant source. Formulas extending their algorithm to the general case of arbitrary range are given in Appendix A, and a pseudocode implementation of the resulting algorithm is given in Appendix B. This implementation was used to investigate the behavior of the transfer function computationally.

Consider first the well-known results for an infinitely distant source (Strutt, 1904). Figure 1 shows a polar plot of $|H(\infty, \mu, \theta)|$ as a function of the angle of incidence for several different frequencies. As Eq. (11) requires, the response at low frequencies is not directionally dependent, with $|H(\infty, \mu, \theta)| \approx 1$ until the normalized frequency nears unity. Above that frequency, the response around the front of the sphere begins to increase noticeably, and the response around most of the back decreases. However, the minimum response does not occur at the very back. Instead, the very back of the sphere exhibits the so-called “bright spot,” which can be explained by arguing that all the waves propagating around the sphere arrive at that point in phase. At very high frequencies, the bright-spot lobe becomes extremely narrow, and the back of the sphere is effectively in a sound shadow. By contrast, the pressure at the front of the sphere is doubled, in agreement with Eq. (12).

Figure 2 shows this same information plotted on a dB scale against normalized frequency for 37 different values of angle of incidence. All of the curves approach 0 dB at low frequencies. The top curve in Fig. 2 shows the 6-dB increase or doubling in magnitude for frontal incidence at high fre-

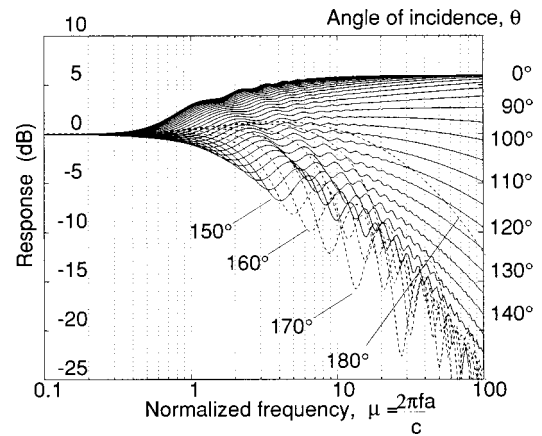


FIG. 2. Magnitude response for an infinitely distant source. Roughly speaking, the response is flat when the angle of incidence is around 100 degrees, exhibits a 6-dB boost at high frequencies near the front of the sphere, and—except for the bright spot at the very back—falls off with frequency around the back of the sphere. Interference effects caused by waves propagating in various directions around the sphere introduce ripples in the response that are quite prominent on the shadowed side.

quencies. The response is approximately 3 dB above the free-field value when the normalized frequency is unity, which supports the statement that the point $\mu=1$ separates low from high frequencies. For the standard 8.75-cm head radius (Hartley and Fry, 1921), this corresponds to about 625 Hz. As the angle of incidence increases, this high-frequency rise changes to a high-frequency rolloff, with the maximum attenuation occurring around $\theta=150$ degrees. The strong interference ripples in the response are visually striking. By contrast, the response at the back of the sphere stays quite flat out to $\mu \approx 20$, which is another manifestation of the bright spot.

B. Frequency response—range dependence

The responses at 0 and 150 degrees can be thought of as providing rough bounds on the frequency response. Figure 3 shows that these bounds separate as the source approaches

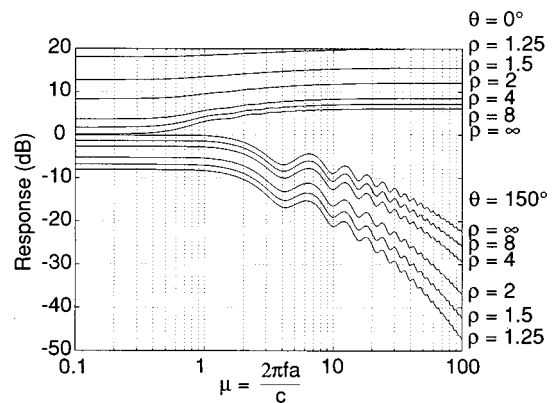


FIG. 3. Effect of range on the magnitude response. (The responses shown are relative to the free-field pressure at the center of the sphere, so that the general inverse range effect is not included.) These curves provide rough bounds on the response at different angles of incidence, with the maximum occurring at $\theta=0$ degrees and the minimum around $\theta=150$ degrees. Note that as the source approaches the sphere, the response increases on the near side and decreases on the far side. This results in the possibility of having large interaural level differences at low frequencies.

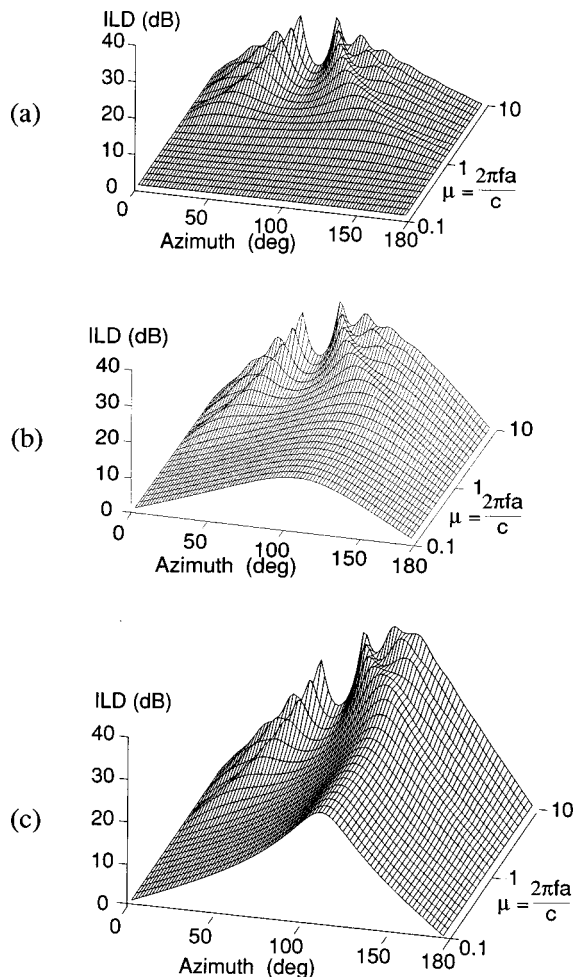


FIG. 4. The interaural level difference (ILD) versus azimuth, assuming that the ears are located at $\theta = \pm 100$ degrees; (a) $\rho = 100$, (b) $\rho = 2$, (c) $\rho = 1.25$. The maximum low-frequency ILD is negligible for a distance source, but becomes quite large as the source approaches the sphere.

the sphere. The response on the near side increases and the response on the far side decreases for all frequencies. It is not surprising that the near-side response gets quite large as the source approaches the sphere, but somewhat less intuitive to see that the response on the far side drops below the free-field response, even at low frequencies.

Another general characteristic is that the difference between the responses at low and high frequencies diminishes on the near side, but increases on the far side. For example, when $\rho = 1.25$, the extra high-frequency rise at the front of the sphere, instead of being 6 dB, is only about 2 dB. This is consistent with the informal experience of a relative increase in the low-frequency content of close sound sources.

These two effects combined imply that the low-frequency interaural level difference (ILD) becomes even further exaggerated as the source approaches one ear. As Blauert (1997) points out, human ears are not located across a diameter, but are set back about 10 degrees. Figure 4(a) shows the ILD for an infinitely distant source, assuming that the “ears” are located at $\theta = \pm 100$ degrees. Note that the ILD is quite small for normalized frequencies below unity. By contrast, when $\rho = 2$, the low-frequency ILD exceeds 10 dB [see Fig. 4(b)], and when $\rho = 1.25$ it exceeds 20 dB [see Fig. 4(c)]. Figure 5 shows that the ILD at an azimuth of 100

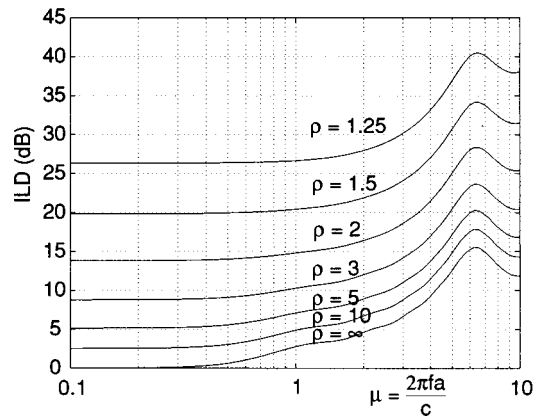


FIG. 5. The ILD when the azimuth to the sound source is 100 degrees. Note that very substantial low-frequency ILD's occur as the source approaches the sphere.

degrees becomes very large as ρ approaches unity, even at low frequencies. This development of a large ILD at low frequencies would seem to be a major cue indicating that a sound source is very close.

C. Impulse response

While the phase response contains useful information about the temporal response, it is more illuminating to invert the transfer function $H(\rho, \mu, \theta)$ and obtain the normalized HRIR $h(\rho, \tau, \theta)$:

$$h(\rho, \tau, \theta) = \int_{-\infty}^{\infty} H(\rho, \mu, \theta) e^{-i2\pi\mu\tau} d\mu, \quad (13)$$

where τ is the normalized time given by³

$$\tau = \frac{ct}{2\pi a}. \quad (14)$$

Figure 6 shows the results of evaluating this integral numerically for the case of an infinitely distant source. Many features of the frequency response are reflected in the impulse response. For example, notice how the amplitude of the pulse drops off and its width increases as the angle of incidence

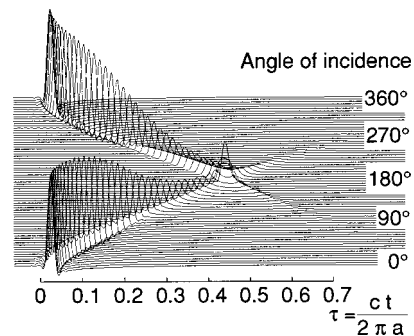


FIG. 6. The theoretical impulse response for an infinitely distant source. The overshoot for small angles of incidence corresponds to the 6-dB boost of high frequencies. As the angle of incidence increases, the pulse is delayed and low-pass filtered by head shadow. Near the back, the effect of waves traveling around the other “side” of the sphere becomes more visible. This is the source of the interference ripples in the magnitude response. The “bright spot” emerges where the various waves arrive at the back of the sphere in phase.

increases, corresponding to the rolloff in response at high frequencies. The overshoot (negative dip in response) that appears for incidence angles below 90 degrees corresponds to the fact that high frequencies are boosted at those angles.

As the angle of incidence approaches 180 degrees, the bright spot becomes prominent in the HRIR. Moreover, the visual appearance of the graph strongly suggests that the impulse “ridge” continues on through the bright spot. One can interpret the overall response as being composed of two ridges, a lower ridge that is due to a wave propagating around one “side” of the sphere, and an upper ridge that is due to a wave propagating around the other “side,” with the bright spot occurring where these two waves join and reinforce one another. Of course, this is a very crude approximation. In particular, adding just these two ridges does not accurately account for either the height of the bright spot or the nearby behavior. However, it explains why the response for incidence angles between 150 and 170 degrees contains two prominent pulses in the time domain, and it qualitatively explains the corresponding pattern of ripples in the frequency domain at all incidence angles.

Figure 7 shows the HRIR for $\rho=1.25$. As one would expect from Fig. 3, as the source is brought closer to the sphere, the response becomes stronger on the near side and weaker and broader on the far side. There is also a difference in the arrival times. In particular, the difference between arrival at the near side and arrival at the far side is smaller at long ranges (Fig. 6) than at close range (Fig. 7).

D. Time delay and minimum-phase reconstruction

There are several ways to define the arrival time of a pulse. While group delay is frequently employed, it is frequency dependent, being significantly greater at low frequencies than at high frequencies (Kuhn, 1977, 1987). With experimentally measured data, it is convenient simply to use $\Delta t_{0.15}$, the time at which the pulse first exceeds 15% of its maximum amplitude; this same definition is used to compute the normalized arrival time for $h(\rho, \tau, \theta)$, $\Delta \tau = c \Delta t_{0.15} / 2\pi a$.

The open circles in Fig. 8 show how this normalized arrival time varies with the angle of incidence for two different normalized ranges, $\rho=1.25$ and $\rho=100$. These two

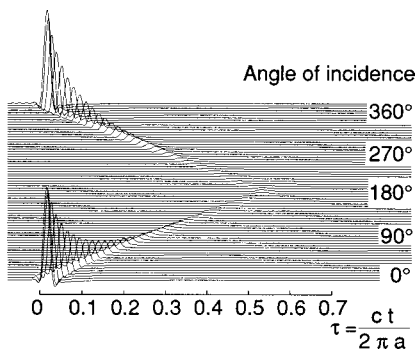


FIG. 7. The theoretical impulse response for a source that is close to the surface of the sphere ($\rho=1.25$). The response drops quite rapidly with azimuth, and the maximum time delay is longer than in Fig. 6.

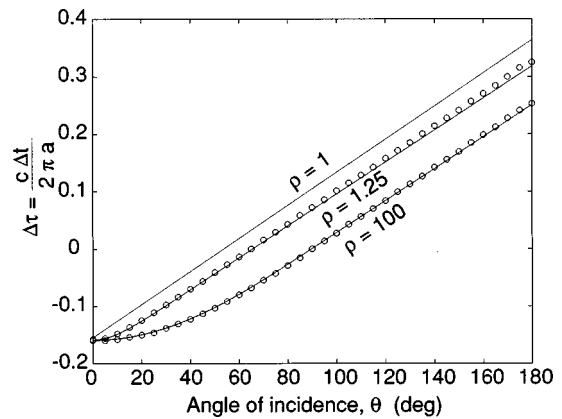


FIG. 8. The delay in arrival time relative to free-field arrival at the center of the sphere. The solid lines are from the Woodworth/Schlosberg ray-tracing formula. The open circles are computed from the theoretical solution as the first time that the impulse response exceeds 15% of its maximum value.

curves are close to the curves for $\rho=1$ and $\rho=\infty$, and thus more or less bound the results at intermediate ranges. Since $\Delta \tau$ is the (normalized) difference between the time of arrival at the surface of the sphere and the free-field time of arrival at the center of the sphere, when the angle of incidence θ is zero, $\Delta \tau$ is negative and is independent of range. At larger incidence angles, $\Delta \tau$ becomes larger as the source approaches the sphere. In addition, the interaural time difference (ITD), which can be computed from $\Delta \tau(\theta+100 \text{ degrees}) - \Delta \tau(\theta-100 \text{ degrees})$, also becomes larger as the source approaches the sphere.

A different method for measuring the time delay was also investigated. Let $h_{mp}(\rho, \tau, \theta)$ be the minimum-phase reconstruction of $h(\rho, \tau, \theta)$. It is well known that minimum-phase reconstruction removes any linear-phase terms associated with pure time delay (Oppenheim and Schaffer, 1989). Indeed, minimum-phase reconstructions are commonly used to time-align impulse responses. When $h_{mp}(\rho, \tau, \theta)$ was computed for many different values of ρ and θ , it was found that, except for time shift, the results were essentially identical to $h(\rho, \tau, \theta)$. The time delay was then computed by maximizing the cross-correlation between $h_{mp}(\rho, \tau, \theta)$ and $h(\rho, \tau, \theta)$. The results were very close to the 15% rise-time results. An interesting byproduct of this investigation was the observation that the HRIR for an ideal sphere appears to be minimum phase for all ranges and incidence angles.

A well-known ray-tracing formula due to Woodworth and Schlosberg (1962) can be extended to get useful approximate equations for the time delay and the ITD (Blauert, 1997, p. 76). As Fig. 9 illustrates, there are two cases, one in which a ray from the source goes directly to the observation point, and one in which the wave must travel from a point of tangency around the sphere to the observation point. If the speed of propagation is assumed to be c both in air and around the surface, a simple geometrical argument shows that the normalized time difference $\Delta \tau$ between the time that the wave reaches the observation point and the time that it would reach the center of the sphere in free field is given by

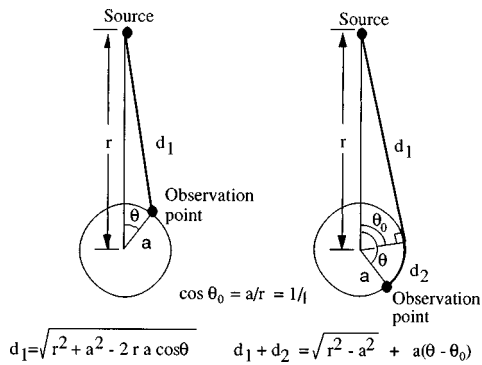


FIG. 9. Geometry for the Woodworth/Schlosberg formula. The wave is assumed to travel with a constant velocity c , whether the distance is the straight line distance d_1 from the source to the observation point, or the sum of distance d_1 from the source to a point of tangency and the distance d_2 around the sphere to the observation point.

$$\Delta \tau = \frac{c \Delta t}{2 \pi a}$$

$$= \begin{cases} \frac{1}{2 \pi} (\sqrt{\rho^2 - 2 \rho \cos \theta + 1} - \rho), & \text{if } 0 \leq \theta \leq \theta_0, \\ \frac{1}{2 \pi} (\theta - \theta_0 + \sqrt{\rho^2 - 1} - \rho), & \text{if } \theta_0 \leq \theta \leq \pi, \end{cases} \quad (15)$$

where

$$\theta_0 = \sin^{-1}(1/\rho), \quad \rho \geq 1. \quad (16)$$

The solid-line curves in Fig. 8 show the predictions of this simple model for $\rho = 1, 1.25$, and ∞ . The agreement with the 15% rise time results is very good, with the maximum error being 2.4% at $\theta = 170$ degrees.

Finally, Fig. 10 shows bounds on the ITD computed from Eqs. (15) and (16) under the assumption that the ears are located at $\theta = \pm 100$ degrees. The upper bound corresponds to a source at the surface of the sphere ($\rho = 1$), and the lower bound corresponds to a source at infinity. Bringing the source closer to the sphere increases the ITD, the maximum increase being 25.7% (0.0908 normalized units, corresponding to 146 μs for the 8.75-cm standard head radius). Brungart and Rabinowitz (1996) obtained essentially the

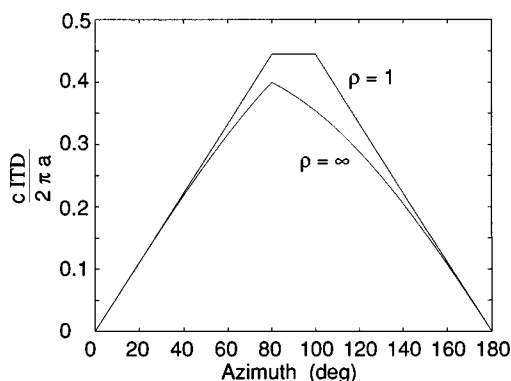


FIG. 10. Bounds on the normalized interaural time difference computed from the Woodworth/Schlosberg formula, assuming that the ears are located at $\theta = \pm 100^\circ$. In general, the ITD is not very sensitive to range.

same results using the phase delay. They pointed out that humans are insensitive to time delays above 700 μs , and the results shown here support their conjecture that changes in the ITD probably do not provide significant information about range.

III. EXPERIMENTAL MEASUREMENTS

The theoretical results presented above are based on assumptions that cannot be met by any physically realizable system (such as the assumption of an ideal point source). Nonetheless, the validity of the basic theory is well established. Although the results of a number of experimental studies of the diffraction of sound by a sphere are reported in the literature, acoustical measurements showing the range dependence of the ILD and ITD were not available. Furthermore, modern techniques for measuring acoustic transfer functions provide a significant improvement over prior techniques, especially in terms of their sensitivity to noise. These considerations led to the following experimental study.

A. Procedure

The response at the surface of a sphere was measured using the same DSP-based techniques currently being employed for measuring human HRTFs. The measurements were made with the Snapshot™ system manufactured by Crystal River Engineering. For each response measurement, this system generated two computer-generated sequences of pseudo-random noise signals called Golay codes. These signals were used to drive a 6.4-cm-diam Bose Acoustimass™ loudspeaker. Signals picked up by the pair of blocked-meatus microphones (typically inserted in the subject's ear canals) were digitized at 44.1 kHz. Snapshot's oneshot function was used to recover the impulse responses without additional compensation or normalization. A record length of 256 samples corresponded to about 5.8 ms and provides a frequency resolution of 172 Hz.

For this study, a single microphone was inserted in a hole drilled through an 3.6-kg, 10.9-cm radius (27-in. circumference) bowling ball. The ball was mounted on a 1.3-cm-diam vertical threaded rod rotated by a motor in 5 degree increments. The ball was positioned in the center of a $5 \times 5 \times 3\text{-m}^3$ anechoic chamber at the University of California at Davis. The center of the ball was 1 m from the chamber floor. Preliminary experiments revealed that the blocked-meatus microphone did not exhibit the expected 6-dB rise at high frequencies, presumably because its 9.5-mm diameter (which is a quarter of a wavelength at 9 kHz) was too large relative to the wavelength. A comparison of the directional variation in the response of the blocked-meatus microphone to that of an Etymotic Research ER-7C probe microphone led to the conclusion that the former exhibited substantial reduction in its response at normal incidence. Thus, the blocked-meatus microphone was replaced by an ER-7C probe microphone. The ER-7C's probe tube was 76 mm long, with a 0.95 mm o.d. and 0.5 mm i.d. The body of the microphone was fully contained within the bowling ball, with the probe tip being flush with the bowling ball's surface.

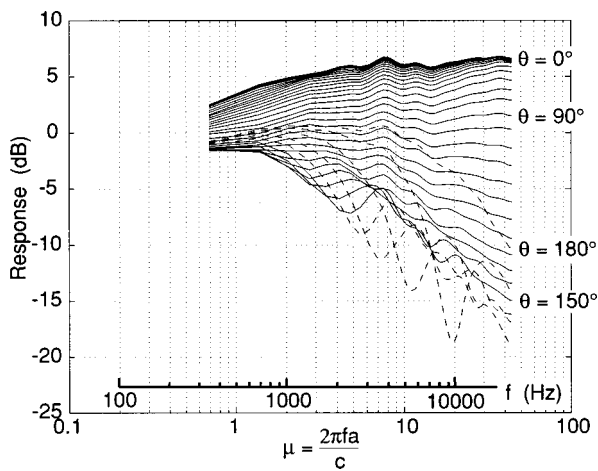


FIG. 11. Experimental measurement of the magnitude response for a 10.9-cm radius bowling ball, $\rho=20$ (cf. Fig. 2). The squared magnitude of the transfer function was smoothed with an auditory filter having a Q of 10.

The loudspeaker, which was mounted on a microphone stand, was located at a distance r from the center of the ball, with the principal axis of the loudspeaker directed at the center of the ball. Measurements were made for $r=13.5, 16, 22, 33, 55, 109,$ and 218 cm, which corresponded to $\rho=1.25, 1.5, 2, 3, 5, 10,$ and 20 , respectively. In addition, free-field measurements were made at each range to allow compensation for the loudspeaker and microphone transfer functions.

B. Measured response

The experimental HRTF was free-field compensated by dividing the FFT of the measured impulse response by the FFT of the free-field response. To reduce the noise and irrelevant fine structure in the measurements, rms values were obtained by smoothing the squared magnitude of the transfer function. A simple constant- Q filter with a Gaussian kernel whose standard deviation was 10% of its center frequency was employed. The resulting frequency response curves for a distant source ($\rho=20$) are shown in Fig. 11. Although there are discrepancies, these results are in general agreement with the theoretical curves shown in Fig. 2. The low-frequency response approaches 0 dB at all incidence angles. At normal incidence ($\theta=0$ degrees), the magnitude response increases with frequency. The response is up about 3 dB at $\mu=1$ and 6 dB at large values of μ . As the angle of incidence increases, the high-frequency response begins to drop off. For $\theta=150$ degrees, the response is down about 13 dB at $\mu=30$, which agrees very well with the theory.

To facilitate comparisons between the theoretical and measured responses, Fig. 12 shows both results for four revealing incidence angles—0, 90, 150, and 180 degrees. Here the theoretical curves are smoothed with the same auditory filter used to smooth the experimental data. Fig. 12(a) is for $\rho=20$, Fig. 12(b) for $\rho=5$, and Fig. 12(c) for $\rho=2$. The results at other ranges are basically similar, and show a good correspondence between theory and measurements. However, for $\rho=1.25$ and $\rho=1.5$ we observed a strong reflection between the ball and the speaker in the vicinity of normal incidence, which produced prominent notches in the 0-

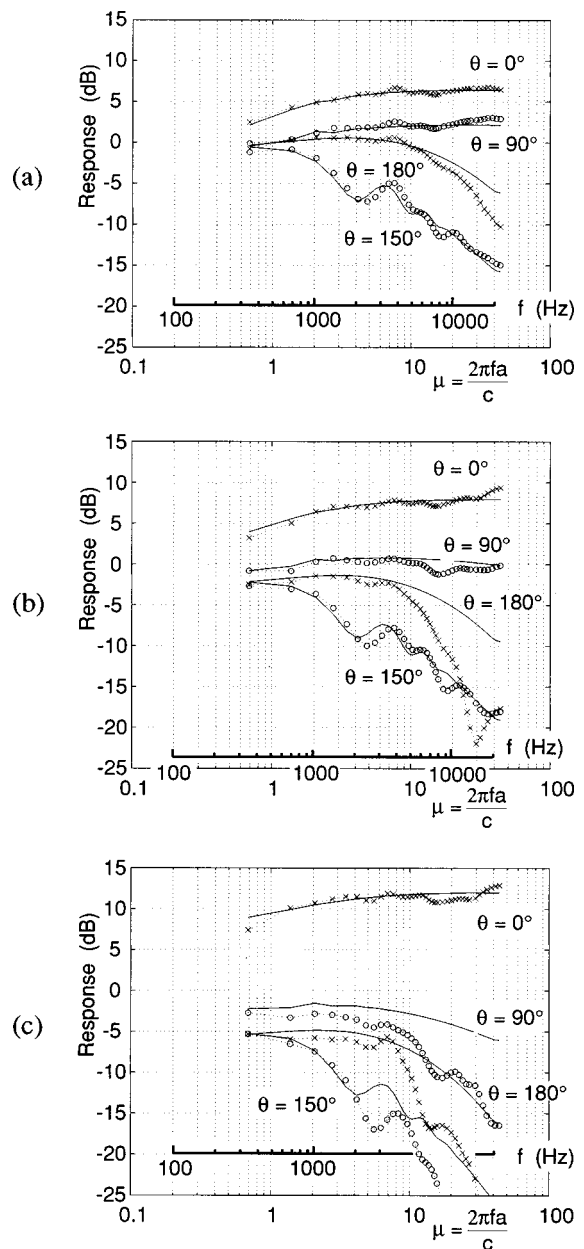


FIG. 12. Comparison between the theoretical and measured responses at four different angles of incidence. (a) $\rho=20$, (b) $\rho=5$, (c) $\rho=2$. For $\rho<2$, the source is no longer well approximated by a point source.

degree curve. Physical sound sources are always spatially extended, and one expects the experimental results to depart from theory at close range.

There are two clear differences between the measured and the theoretical results that appear in all of the ranges measured. The first is that there are discrepancies between the ripple patterns above 2 kHz. This is probably due to small angular errors, since the frequencies at which the interference effects occur are quite sensitive to the angle of incidence. The second is a reduction in the measured high-frequency response at $\theta=180$ degrees, which reduces the strength of the bright spot. This is also probably due to small alignment errors, plus the presence of the supporting rod, the exiting microphone cable, and other imperfections that disturb the wave propagation from what would occur with a perfect sphere. These discrepancies could undoubtedly be re-

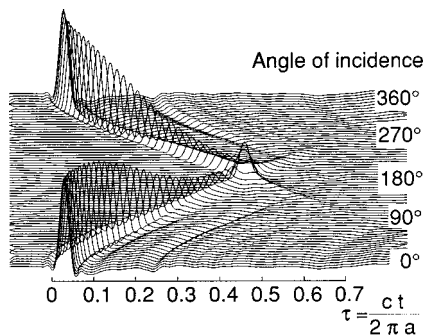


FIG. 13. Experimental measurement of the impulse response for a 10.9-cm radius bowling ball, $\rho=20$ (cf. Fig. 6). The smaller waves following the main pulse are probably due to reflections within the ball.

duced by more careful experimental techniques. However, extremely controlled conditions are not feasible for human HRTF measurements. Since human heads, necks and torsos introduce much greater perturbations, it is not surprising that phenomena such as bright spots that depend critically on geometry can be overlooked in human HRTF measurements.

Figure 13 shows the HRIR obtained by inverse transforming the free-field-compensated HRTF for $\rho=20$ and interpolating by a factor of 4 to smooth the curves. Again, the results are basically similar to the theoretical predictions (cf. Fig. 6). The amplitude of the pulse drops off and broadens in the same way, and a bright spot in fact appears where the two “ridges” cross. The visually most prominent difference between experiment and theory appears in the fairly large number of low-amplitude waves that follow the primary response. These are probably due to reflections caused by waves propagating through the interior of the bowling ball.

Figure 14 shows the time delay computed from the experimentally measured HRIR’s using the 15% rise-time definition for the cases $\rho=2$ (open circles) and $\rho=20$ (x’s). As in Fig. 8, the solid lines are computed using Woodworth and Schlosberg’s approximate formula. Once again, this simple formula provides a very good approximation.

IV. DISCUSSION

There is a long history of research on the diffraction of sound by a rigid sphere that dates back at least to the classi-

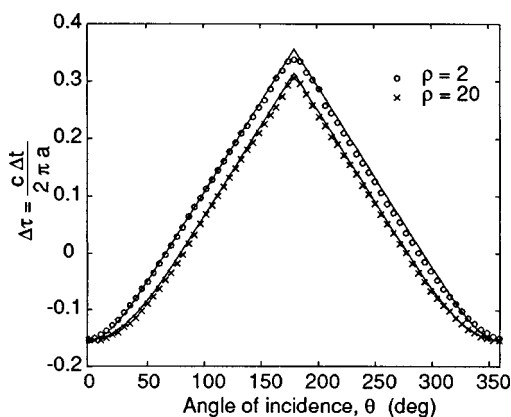


FIG. 14. Comparison of arrival times as measured from the impulse response and calculated by Woodworth and Schlosberg’s formula.

cal work by Lord Rayleigh (Strutt, 1904, 1945). Hartley and Fry (1921) presented theoretical graphs showing the azimuth and range dependence of the ILD and the interaural phase difference (IPD). They conjectured that the auditory system could determine both the azimuth and the range for the source of a pure tone from the ILD and the IPD taken jointly. Wightman and Firestone (1930) tested this conjecture experimentally, and reported that people were unable to judge the distance to pure tones from this information. Similar failures were later reported by Coleman (1962). Without referring to this earlier work, Hirsch (1968) used a simple inverse-square approximation to show that, in theory, the range to a source could be determined from the ratio of the interaural time difference to a percentage interaural intensity difference. Molino (1973) refined Hirsch’s analysis, but again found that human subjects were unable to distinguish five different amplitude normalized sources at ranges of 3 to 38 ft when pure tones (1000 and 8000 Hz) were used.

It is now understood that such dry, narrow-band stimuli usually do not produce images of auditory events that are heard as external to the listener’s head, and so distance judgments will be particularly difficult for subjects to make. The issue of externalization is critically important to psychophysical studies of the apparent distance of stimuli presented via headphones. Not only are wideband signals needed for good directional judgments, but the inclusion of indirect sound (reflections and/or reverberation) is also required for the best externalization (Durlach *et al.*, 1992). Without psychophysical studies of apparent distance employing adequate stimuli, it is difficult to discuss further the importance of the range dependence of the ILD and the IPD in human distance perception.

Earlier work has also been done on comparing acoustical measurements and diffraction theory. Wiener (1947) provided experimental verification of Rayleigh’s solution for an infinitely distant source by measuring the pressure at the surface of a smoothly finished 9.7-cm-radius wooden sphere in an anechoic chamber. He used a probe microphone and a sinusoidal source located about 2 m from the center of the sphere. While Wiener’s results exhibit considerable variability and do not include range dependence, they do confirm the basic features of the theoretical solution. For the case of an infinitely distant source, Feddersen *et al.* (1957) experimentally confirmed the accuracy of Woodworth and Schlosberg’s formula for the ITD, and Kuhn (1977, 1987) used the phase response to derive the ITD from Rayleigh’s solution. Rabinowitz *et al.* (1993) presented the range-dependent theoretical solution. Brungart and Rabinowitz (1996) subsequently used this result to determine both the ILD and the ITD as functions of range, and observed that while the ILD varies strongly with range, the ITD is not very sensitive to range.

The results reported in this paper extend this earlier work by presenting an algorithm for computing both the HRTF and the HRIR for any range and angle of incidence, and by confirming these results experimentally. The time-domain results illuminate the somewhat puzzling character of the bright spot, and the ripples that appear in the frequency response in the vicinity of the bright spot. Although

it is an oversimplification to say that these phenomena are due to two waves propagating around the two “sides” of the sphere, this interpretation provides a simple and useful first approximation.

V. CONCLUSIONS

To summarize, both the theoretical and experimental data confirm that the variation of low-frequency ILD with range is significant for ranges smaller than about five times the sphere radius. The impulse response provides direct evidence that the ITD is not a strong function of range. The time delay is well approximated by the well-known ray-tracing formula due to Woodworth and Schlosberg. Finally, except for this time delay, the HRTF for the ideal sphere appears to be minimum phase, permitting exact recovery of the impulse response from the magnitude response in the frequency domain.

ACKNOWLEDGMENTS

We are grateful to Professor V. R. Algazi at the University of California at Davis for his help in measuring the experimental data. Intel Corporation donated the probe microphones used to make our experimental measurements. The material in this paper is based upon work supported by the National Science Foundation under Grant Nos. IRI-9402246 and IRI-9619339. Any opinions, findings, and conclusions or recommendations expressed in this material are those of the authors and do not necessarily reflect the views of the National Science Foundation.

APPENDIX A: RECURSION RELATIONS

The basis for the algorithm by Bauch and Cooper (1980) is the following recursion relation for spherical Hankel functions (Morse and Ingard, 1968, Chap 7.2):

$$h_m(x) = \frac{2m-1}{x} h_{m-1}(x) - h_{m-2}(x), \quad m=2,3,\dots, \quad (\text{A1})$$

where

$$h_0(x) = \frac{e^{ix}}{ix} \quad \text{and} \quad h_1(x) = -i \left[\frac{1}{ix} - \frac{1}{(ix)^2} \right] e^{ix}. \quad (\text{A2})$$

The computation of $h_m(x)$ can be significantly simplified by defining an auxiliary function $Q_m(z)$ through the equation

$$h_m(x) = Q_m\left(\frac{1}{ix}\right) (-i)^m e^{ix}. \quad (\text{A3})$$

It is not hard to show that $Q_m(z)$ satisfies the recursion equation

$$Q_m(z) = -(2m-1)zQ_{m-1}(z) + Q_{m-2}(z), \quad m=2,3,\dots, \quad (\text{A4})$$

where

$$Q_0(z) = z \quad \text{and} \quad Q_1(z) = z - z^2. \quad (\text{A5})$$

Thus, $Q_m(z)$ is a simple polynomial in z that can easily be computed recursively. Furthermore, by using the recursion relation (see Morse and Ingard, 1968, Chap 7.2)

$$h'_m(x) = \frac{1}{2m+1} [mh_{m-1}(x) - (m+1)h_{m+1}(x)], \quad (\text{A6})$$

one can employ Eqs. (A1) and (A3) to obtain

$$h'_m(x) = \left[Q_{m-1}\left(\frac{1}{ix}\right) - \frac{m+1}{ix} Q_m\left(\frac{1}{ix}\right) \right] (-i)^{(m-1)} e^{ix}, \quad (\text{A7})$$

where the case $m=1$ can be included by defining $Q_{-1}(z) = z$. Thus, the derivative of the spherical Hankel function can also be computed directly from the Q polynomials. In addition, the Legendre polynomials can also be computed recursively through

$$P_m(x) = \frac{2m-1}{m} x P_{m-1}(x) - \frac{m-1}{m} P_{m-2}(x), \quad (\text{A8})$$

where

$$P_0(x) = 1 \quad \text{and} \quad P_1(x) = x. \quad (\text{A9})$$

Finally, by combining Eqs. (7), (8), (A3), and (A7), we obtain

$$H(\rho, \mu, \theta) = \frac{\rho}{i\mu} e^{-i\mu} \sum_{m=0}^{\infty} (2m+1) P_m(\cos\theta) \times \frac{Q_m(1/i\mu\rho)}{\frac{m+1}{i\mu} Q_m\left(\frac{1}{i\mu}\right) - Q_{m-1}\left(\frac{1}{i\mu}\right)}, \quad \rho > 1, \quad (\text{A10})$$

where the complex polynomials P_m and Q_m are computed recursively through Eqs. (A4), (A5), (A8), and (A9). An algorithm based on these relations that can be converted directly into a MATLAB[®] or a Mathematica[™] program is given in Appendix B.

APPENDIX B: THE HRTF ALGORITHM

The following pseudo-code defines an algorithm for evaluating Eq. (A10). It assumes that variables and expressions can have complex values. The first two terms in the series are explicitly computed, and the use of recursion starts with $m=3$. Iteration stops when the fractional change falls below a user-supplied threshold for two successive terms.

```

function H = sphere(a, r, theta, f, c, threshold)
    x = cos(theta);
    mu = (2 * pi * f * a) / c;
    rho = r / a;
    i = sqrt(-1);
    zr = 1 / (i * mu * rho);
    za = 1 / (i * mu);
    Qr2 = zr;
    Qr1 = zr * (1 - zr);
    Qa2 = za;
    Qa1 = za * (1 - za);
    P2 = 1;
    P1 = x;
    sum = 0;
    term = zr / (za * (za - 1));
    sum = sum + term;
    term = (3 * x * zr * (zr - 1)) / (za * (2 * za2 - 2 * za + 1));
    sum = sum + term;
    oldratio = 1; newratio = abs(term)/abs(sum);
    m = 2;
    while (oldratio > threshold) or (newratio > threshold),
        Qr = - (2 * m - 1) * zr * Qr1 + Qr2;
        Qa = - (2 * m - 1) * za * Qa1 + Qa2;
        P = ( (2 * m - 1) * x * P1 - (m - 1) * P2) / m;
        term = ( (2 * m + 1) * P * Qr) / ( (m + 1) * za * Qa - Qa1);
        sum = sum + term;
        m = m + 1;
        Qr2 = Qr1; Qr1 = Qr; Qa2 = Qa1; Qa1 = Qa; P2 = P1; P1 = P;
        oldratio = newratio; newratio = abs(term)/abs(sum);
    end while;
    H = (rho * exp(- i * mu) * sum) / (i * mu);
end function;

```

¹See Morse and Ingard (1968, Chap 7). Because we use $e^{i(kr - \omega t)}$ instead of $e^{i(\omega t - kr)}$ to represent a traveling wave, our formulas agree with those in Morse and Ingard (1968) and in Bauck and Cooper (1980), but are the complex conjugates of the formulas in Kuhn (1977) and in Rabinowitz *et al.* (1993).

²The classical HRTF relates the pressure at the source to the pressure at the head. While the pressure at an ideal point source is infinite, the pressure p_e at a small sphere of radius r_e surrounding the source is approximately $[(-i\omega\rho_0 S_\omega)/(4\pi r_e)]e^{i\omega t}$. The transfer function H_e from this small sphere to the diffracting sphere is given by

$$H_e = \frac{p_s}{p_e} = \frac{p_s p_{ff}}{p_{ff} p_e} = H \frac{r_e}{r} e^{ikr} = H \frac{r_e}{r} e^{i\omega(r/c)}$$

In the time domain, the phase factor $e^{i\omega(r/c)}$ corresponds to the propagation delay of r/c . Thus, except for the uninteresting constant scale factor r_e , one can use H to find the classical HRTF H_e merely by adding the effects of propagation delay and dividing by the range.

³It should be noted that the time scaling of the impulse response function also leads to amplitude scaling. Thus, the unnormalized impulse response is given by $\hat{h}(r, t, \theta) = (c/2\pi a)h(r/a, ct/2\pi a, \theta)$. This amplitude scaling guarantees that the area under the impulse response is the dc value of the transfer function.

Bauck, J. L., and Cooper, D. H. (1980). "On acoustical specification of natural stereo imaging," Preprint 1649 (H-7), 66th Convention Audio Engineering Society, Los Angeles, CA.

Blauert, J. (1997). *Spatial Hearing* (revised edition) (MIT, Cambridge, MA). Original edition published as *Räumliches Hören* (Hirzel, Stuttgart, Germany, 1974).

Brungart, D. S., and Rabinowitz, W. R. (1996). "Auditory localization in the near field," Proc. ICAD 96 (Third International Conference on Auditory Display), Palo Alto, CA (<http://www.santafe.edu/~icad/ICAD96/proc96/INDEX.HTM>).

Coleman, P. D. (1962). "Failure to localize the source distance of an unfamiliar sound," J. Acoust. Soc. Am. **34**, 345–346.

Durlach, N. I., Rigopulos, A., Pang, X. D., Woods, W. S., Kulkarni, A., Colburn, H. S., and Wenzel, E. M. (1992). "On the externalization of auditory images," Presence **1**, 251–257.

Feddersen, W. E., Sandel, T. T., Teas, D. C., and Jeffress, L. A. (1957). "Localization of high-frequency tones," J. Acoust. Soc. Am. **29**, 988–991.

Hartley, R. V. L., and Fry, T. C. (1921). "The binaural localization of pure tones," Phys. Rev. **18**, 431–442.

Hirsch, H. R. (1968). "Perception of the range of a sound source of unknown strength," J. Acoust. Soc. Am. **43**, 373–374.

Kuhn, G. F. (1977). "Model for the interaural time differences in the azimuthal plane," J. Acoust. Soc. Am. **62**, 157–167.

Kuhn, G. F. (1987). "Physical acoustics and measurements pertaining to directional hearing," in *Directional Hearing*, edited by W. A. Yost and G. Gourevitch (Springer-Verlag, New York), pp. 3–25.

Molino, J. (1973). "Perceiving the range of a sound source when the direction is known," J. Acoust. Soc. Am. **53**, 1301–1304.

Morse, P. M., and Ingard, K. U. (1968). *Theoretical Acoustics* (Princeton U.P., Princeton, NJ).

Oppenheim, A. V., and Schaffer, R. W. (1989). *Discrete-Time Signal Processing* (Prentice-Hall, Englewood Cliffs, NJ).

- Rabinowitz, W. M., Maxwell, J., Shao, Y., and Wei, M. (1993). "Sound localization cues for a magnified head: Implications from sound diffraction about a rigid sphere," *Presence* **2**, 125–129.
- Strutt, J. W. (Lord Rayleigh) (1904). "On the acoustic shadow of a sphere," *Philos. Trans. R. Soc. London, Ser. A* **203**, 87–89.
- Strutt, J. W. (Lord Rayleigh) (1945). *The Theory of Sound* (Dover, New York), 2nd ed., Vols. 1 and 2.
- Wiener, F. M. (1947). "Sound diffraction by rigid spheres and circular cylinders," *J. Acoust. Soc. Am.* **19**, 444–451.
- Wightman, E. R., and Firestone, F. A. (1930). "Binaural localization of pure tones," *J. Acoust. Soc. Am.* **2**, 271–280.
- Woodworth, R. S., and Schlosberg, G. (1962). *Experimental Psychology* (Holt, Rinehard and Winston, New York), pp. 349–361.